

Authors: Scott Zolkos*, Suzanne E. Tank

Affiliation: Department of Biological Sciences, University of Alberta, Edmonton, AB, T6G 2E3, Canada

Contact: zolkos@ualberta.ca

1. Introduction and Contents

This project investigates thermokarst effects on land-water linkages and biogeochemical cycling on the Peel Plateau (Northwest Territories, Canada). As part of this project, samples were collected in July 2017 from permafrost exposures at eight retrogressive thaw slump features (RTSs) and the morphology of RTSs was measured. The Peel Plateau region and RTSs are described in detail in the literature (Kokelj et al., 2017; Lacelle et al., 2015; Littlefair et al., 2017; St. Pierre et al., 2018; Zolkos et al., 2018).

This file contains detailed field and laboratory methods, site photographs, and the raw data for RTS morphology measurements. Geochemistry samples were collected, processed in a field laboratory, and analyzed at expert laboratories following standard procedures.

2. Methods

2.1. Field Methods

During summer 2017 (July 10–17), we sampled permafrost and rill runoff thaw streams at eight retrogressive thaw slump (RTS) features. We selected RTSs exposing varying proportions of the Holocene and Pleistocene stratigraphic layers, to consider geochemical effects associated with RTS morphology (Littlefair et al., 2017). These layers were differentiated in the field based on stratigraphy and in the lab using stable isotopes in water ($\delta^{18}\text{O}$, $\delta^2\text{H}$) (Lacelle et al., 2013; Michel, 2011). Permafrost samples were collected using a mallet and stainless-steel chisel. The outer 5-10 cm of exposed permafrost was removed prior to sampling and all samples were stored in 5L Whirlpak bags. Runoff was collected in triple sample-rinsed 2L HDPE bottles, stored cool and dark, and refrigerated (4°C, dark) upon returning from the field. Runoff was processed within 24h for all parameters except stable isotopes in water, which were filtered in the field. Silicon in runoff was collected without headspace in triple sample-rinsed 30 mL HDPE bottles, sealed with electrical tape, and stored cool and dark until analysis.

To characterize RTS morphology, we measured headwall height at the time of sampling using a Uineye HK1200 laser range finder (± 30 cm/0.35° accuracy). A handheld GPS unit (Garmin GPSMAP 64ST, ± 3.65 m accuracy) was used to determine the coordinates of the point at which morphology measurements were made.

2.2. Laboratory Methods

Permafrost samples were thawed in coolers and the supernatant was collected and filtered for stable isotopes in water and general chemistry. All subsamples were refrigerated until analysis, except for dissolved inorganic nitrogen (DIN; ΣNH_4^+ , NO_3^- , NO_2^- ; stored at -15°C), and were filtered using 0.45- μm cellulose acetate filters (except DOC [polyethersulfone, PES]). Filters were flushed with 5 mL of filtrate before subsampling.

Stable isotopes in water were filtered into 2 mL glass vials without headspace and analyzed at the University of Alberta Biogeochemical Analytical Services Laboratory (BASL) by cavity ringdown spectroscopy (Picarro L2130-i). Isotope ratios were determined from calibration curves built from U.S. Geological Survey secondary standards (USGS45 and USGS46) and in-house tap water, calibrated by an International Atomic Energy Agency standard as a quality control.

Cations and trace metals were filtered using acid washed (24h, 10% HCl by volume) all-plastic syringes and acidified with trace metal-grade HNO_3 . Samples were measured at the BASL by Inductively-Coupled Argon Plasma Optical Emission Spectrometer (Thermo ICAP-6300).

Anions were filtered into non-acid washed 15 mL polypropylene centrifuge tubes and analyzed at the BASL by Ion Chromatography (Dionex DX-600).

Dissolved organic carbon (DOC) was filtered into precombusted (5h, 500°C) glass vials and acidified to $\text{pH} < 2$ using trace metal-grade HCl. DOC was measured by high-temperature combustion (Shimadzu 5000A TOC Analyzer), using a four-point standard curve prepared from KHP standard solutions (ACCUSPEC). An in-house caffeine standard (10 mg L^{-1}) was analyzed every 20 samples to monitor instrument drift.

UV-visible absorbance was analyzed in a field lab at room temperature within one week. Samples were analyzed in duplicate using an Ocean Optics UV-VIS instrument with a Flame spectrometer module and 1 cm quartz cuvette. MilliQ water blanks were analyzed every 10 samples to monitor machine drift. For each sample, the absorbance at 750 nm was used to correct for offset due to scattering (Stubbins et al., 2017). We additionally corrected the spectra for Fe interference (Poulin et al., 2014) and, using the corrected spectra, we calculated specific UV absorbance at 254 nm (SUVA_{254} , $\text{L mgC}^{-1} \text{ m}^{-1}$) as the Decadic absorption coefficient at 254 nm (A_{254} , m^{-1}) divided by DOC concentration (Weishaar et al., 2003). The slope ratio (S_R), which can be a useful indicator of DOC molecular weight, was calculated following Helms et al. (2008).

Permafrost geochemistry and retrogressive thaw slump morphology (Peel Plateau, Canada)
Supplementary Material

TDN and DIN were filtered into acid washed, 60 mL HDPE bottles and 15 mL polypropylene centrifuge tubes, respectively. All nitrogen species and Si were analyzed at BASL by flow injection analysis (Lachat QuickChem QC8500 FIA Automated Ion Analyzer). NO_3^- and NO_2^- concentrations were determined using automated colorimetry. DON was calculated as the difference between TDN and DIN.

Data below the minimum detection limit are reported as <MDL.

3. Detailed Site Information and Photos

For additional and/or high-resolution photos, contact Scott Zolkos (zolkos@ualberta.ca)



Fig S1. FM2 (photo date: July 9, 2014). Note: photo depicts one of the several lobes of RTS FM2. FM2 is among the largest, oldest, and most rapidly growing RTS features on the Peel Plateau (headwall retreat rate = 15 m y^{-1} ; Lacelle et al., 2015). The permafrost headwall of FM2 is a massive exposure of deformed, layered ice-rich sediments and the debris tongue was ~ 1.6 km in 2017. See also Kokelj et al. (2013), Lacelle et al. (2013), Littlefair et al. (2017), Malone et al. (2013), van der Sluijs et al. (2018), and Zolkos et al. (2018).



Fig S2. FM3 (photo date: July 13, 2017). FM3 is a well-documented RTS feature situated 1.5 km north of Dempster Highway. See also Kokelj et al. (2013), Lacelle et al. (2013), Littlefair et al. (2017), Malone et al. (2013), van der Sluijs et al. (2018), and Zolkos et al. (2018).



Fig S3. SD (photo date: July 13, 2017). SD is located 600 m north of Dempster Highway. SD may have formed within the last 10 years, perhaps as a secondary feature following thermo-erosion by a creek that was diverted by the growing debris tongue of the larger RTS feature immediately to the west (S.V. Kokelj, *personal communication*). See also Littlefair et al. (2017) and Zolkos et al. (2018).



Fig S4. SE (photo date: August 21, 2015). SE is located ~3.2 km south of Dempster Highway. SE has grown rapidly since 2015. Landsat satellite imagery suggest it is at least 15-20 years old (S. Zolkos, unpublished data; see also St. Pierre et al., 2018; Zolkos et al., 2018).



Fig S5. SF (photo date: July 10, 2017). SF is located ~100 m north of Dempster Highway at base of Richardson Mountains. No published age or growth rate.



Fig S6. SG (photo date: July 10, 2017). SG is located ~300 m south of Dempster Highway, ~7 km west of Midway Lake on the Peel Plateau. No published age or growth rate.



Fig S7. HC (photo date: July 17, 2017). HC is 17 km north of Dempster Highway. Analysis of Landsat imagery suggests the HC scar zone nearly doubled in area to ~2.5 ha and its headwall retreated ~30–70 m between 2010 and 2017 (S. Zolkos, unpublished data). See also Littlefair et al. (2017).



Fig S8. HD (photo date: July 17, 2017). HD is 18 km north of Dempster Highway. Field observations suggest the Holocene permafrost at HD is relatively more peat-rich than at the other sites. In 2015, we recovered sulfide-bearing rock from the debris tongue of HD and observed iron oxides deposited on the debris tongue. See also Littlefair et al. (2017), St. Pierre et al. (2018), and Zolkos et al. (2018).

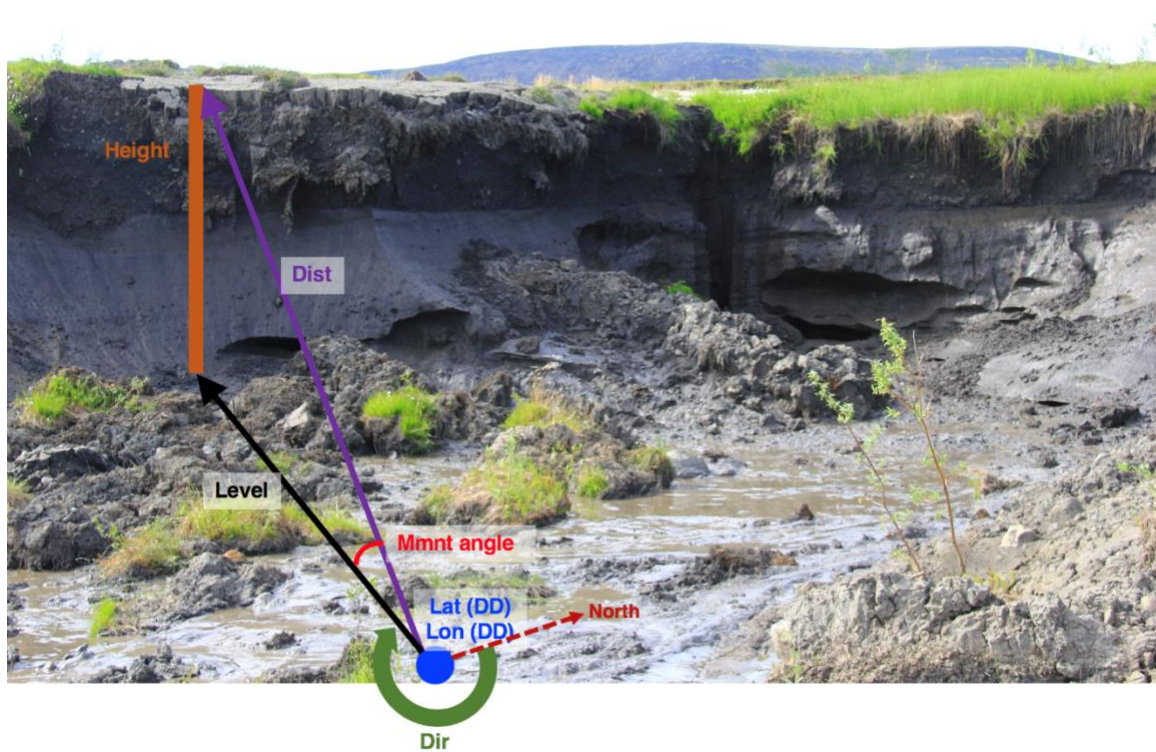


Fig S9. Diagram illustrating the data collected for each retrogressive thaw slump morphology measurement (see Table S1).

Supplementary Material

Table S1. Coordinates of Holocene (HO) and Pleistocene (PL) permafrost and runoff (RU) sampling locations, and location from which measurements of retrogressive thaw slump morphology were made (morph). Dir = compass direction (in degrees) of morphology measurement (not corrected for magnetic declination); Angle = angle (in degrees) of range measurement of headwall height (i.e. above imaginary horizontal plane); Dist = distance (meters) from laser range finder to measurement point at top of headwall; Level = horizontal distance (meters) from laser range finder to headwall measurement point; height = headwall height (m).

Site	Date	Source	Lat (DD)	Lon (DD)	Dir (°)	Angle (°)	Dist (m)	Level (m)	Height (m)
FM2	7/12/17	FM2-HO	67.25326	-135.23495					
		FM2-PL	67.25786	-135.22745					
		FM2-RU	67.25984	-135.23590					
		FM2-morph 1	67.25711	-135.22891					
		1			327	1	135.9	136	2.8
		2			323	1.1	127.3	127.1	2.8
		3			330	1.2	140.6	139.8	3.1
		FM2-morph 2	67.25711	-135.22891					
		1			28	2.4	121.4	123.4	5.8
		2			14	2.5	119.2	118.7	6.2
		3			25	2.4	121.4	120.9	6.2
		FM2-morph 3	67.25711	-135.22891					
		7			155	4	173.5	172.1	13.5
		8			158	4	171.4	170	11.2
		9			146	4	169.8	168.2	15.4
FM2-morph 4	67.25354	-135.23482							
1			212	13.2	20.6	20.3	3.6		
FM2-morph 5	67.25298	-135.23425							
1			168	6.9	102	102	9.5		
2			148	10.1	164.6	163.9	24.2		
3			130	3.8	307.7	305	21.4		
4			129	3.2	329.7	334	21.7		
5			110	2.1	376.1	376	16.1		

Permafrost geochemistry and retrogressive thaw slump morphology (Peel Plateau, Canada)

Supplementary Material

					Mean height:		10.90		
FM3	7/13/17	FM3-HO	67.25542	-135.27232					
		FM3-PL	67.25579	-135.27539					
		FM3-RU	67.25183	-135.27174					
		FM3-morph 1	67.25525	-135.27469					
		1			224	2.4	105.6	105.2	4.5
		2			259	4.9	105.8	105.3	9.1
		3			304	7.3	68.6	67.8	9.8
		4			355	3.9	84.6	83.9	6
		5			25	2.3	123.4	122.9	5.2
		6			55	1.5	132.8	132.5	4.2
					Mean height:		6.47		
SD	7/13/17	SD-HO	67.18065	-135.72694					
		SD-PL	67.18204	-135.72870					
		SD-RU	67.18121	-135.72720					
		SD-morph 1	67.18169	-135.72891					
		1			274	9.8	355	35.3	5.1
		2			308	7.8	44.8	44.3	3.6
		3			260	7.2	52.1	51.9	3.4
		4			234	8.5	43.6	43.4	5.8
		5			215	4	55.4	54.8	3.6
		SD-morph 2	67.18095	-135.72777					
		1			38	3.5	47.4	47.4	2.9
		2			30	3.2	57.8	57.7	3.2
		SD-morph 3	67.18046	-135.72749					
		1			54	5.3	29.3	29.2	2.6
		2			115	6.2	21.9	22.1	2.1
					Mean height:		2.70		

Permafrost geochemistry and retrogressive thaw slump morphology (Peel Plateau, Canada)

Supplementary Material

SE	7/14/17	SE-HO	67.14804	-135.71944					
		SE-PL	67.14796	-135.71939					
		SE-RU	67.14864	-135.71870					
		SE-morph 1	67.14833	-135.71904					
		1			200	6.3	49.6	49	6.4
		2			179	5.4	154.9	151.3	21.2
		3			162	6	175.1	172.7	24.0
		4			148	6.7	172	169.4	21.5
		5			136	4.9	163.4	162.1	16.5
Mean height: 17.92									
SF	7/10/17	SF-HO	67.18296	-135.81065					
		SF-PL	67.18297	-135.81076					
		SF-RU	67.18319	-135.80994					
		SF-morph 1	67.18318	-135.81027					
		1			250	11.2	44.3	43.3	7.6
		2			278	11.2	36.3	35.3	6.7
		3			310	8.1	16.8	16.6	1.8
		4			233	8.8	40.1	39.5	6.2
Mean height: 5.58									
SG	7/10/17	SG-HO	67.21223	-135.59778					
		SG-PL	67.21226	-135.59753					
		SG-RU	N/A	N/A					
		SG-morph 1	67.21231	-135.59790					
		1			102	9.2	17.2	17	2.7
		2			122	7.8	15.6	15.6	2.1
		3			158	5.2	13.3	13.2	1.2
		4			82	4.8	17.2	17.1	2.7
		5			48	7.7	16.2	16.1	2.2

Permafrost geochemistry and retrogressive thaw slump morphology (Peel Plateau, Canada)

Supplementary Material

					Mean height:		2.18		
HC	7/17/17	HC-HO	67.32875	-135.90024					
		HC-PL	67.32848	-135.90007					
		HC-RU	67.32751	-135.89799					
		HC-morph 1	67.32835	-135.89987					
		1			161	2.5	181	180.8	8.6
		2			178	10.1	103.7	102.7	18.3
		3			208	22.8	40.2	37.7	16.2
		4			232	25.5	36.9	34.5	14.2
		5							9.4
		5a			300	7.2	23.9	23.8	3.2
		5b			307	7.4	43.7	42.2	6.2
					Mean height:		13.34		
HD	7/17/17	HD-HO	67.39991	-135.33240					
		HD-PL	67.40005	-135.33310					
		HD-RU	67.40085	-135.33553					
		HD-morph 1	67.40041	-135.33208					
		1			19	1.5	98.1	97.9	3.1
		2			42	11.1	67.6	66.3	13.6
		3			169	12.7	46.2	45.6	6.7
		4			62	14.1	48.5	46.3	10.7
					Mean height:		8.53		

Supplementary references

- Helms, J. R., Stubbins, A., Ritchie, J. D., Minor, E. C., Kieber, D. J., & Mopper, K. (2008). Absorption spectral slopes and slope ratios as indicators of molecular weight, source, and photobleaching of chromophoric dissolved organic matter. *Limnology and Oceanography*, *53*(3), 955–969. <https://doi.org/10.4319/lo.2008.53.3.0955>
- Kokelj, S. V., Lacelle, D., Lantz, T. C., Tunnicliffe, J., Malone, L., Clark, I. D., & Chin, K. S. (2013). Thawing of massive ground ice in mega slumps drives increases in stream sediment and solute flux across a range of watershed scales. *Journal of Geophysical Research: Earth Surface*, *118*(2), 681–692. <https://doi.org/10.1002/jgrf.20063>
- Kokelj, S. V., Tunnicliffe, J. F., & Lacelle, D. (2017). The Peel Plateau of Northwestern Canada: An Ice-Rich Hummocky Moraine Landscape in Transition. In O. Slaymaker (Ed.), *Landscapes and Landforms of Western Canada* (pp. 109–122). Cham: Springer International Publishing. https://doi.org/10.1007/978-3-319-44595-3_7
- Lacelle, D., Lauriol, B., Zazula, G., Ghaleb, B., Utting, N., & Clark, I. D. (2013). Timing of advance and basal condition of the Laurentide Ice Sheet during the last glacial maximum in the Richardson Mountains, NWT. *Quaternary Research*, *80*(02), 274–283. <https://doi.org/10.1016/j.yqres.2013.06.001>
- Lacelle, D., Brooker, A., Fraser, R. H., & Kokelj, S. V. (2015). Distribution and growth of thaw slumps in the Richardson Mountains–Peel Plateau region, northwestern Canada. *Geomorphology*, *235*, 40–51. <https://doi.org/10.1016/j.geomorph.2015.01.024>
- Littlefair, C. A., Tank, S. E., & Kokelj, S. V. (2017). Retrogressive thaw slumps temper dissolved organic carbon delivery to streams of the Peel Plateau, NWT, Canada. *Biogeosciences*, *14*(23), 5487–5505. <https://doi.org/10.5194/bg-14-5487-2017>
- Malone, L., Lacelle, D., Kokelj, S., & Clark, I. D. (2013). Impacts of hillslope thaw slumps on the geochemistry of permafrost catchments (Stony Creek watershed, NWT, Canada). *Chemical Geology*, *356*, 38–49. <https://doi.org/10.1016/j.chemgeo.2013.07.010>
- Michel, F. A. (2011). Isotope characterisation of ground ice in northern Canada. *Permafrost and Periglacial Processes*, *22*(1), 3–12. <https://doi.org/10.1002/ppp.721>
- Poulin, B. A., Ryan, J. N., & Aiken, G. R. (2014). Effects of Iron on Optical Properties of Dissolved Organic Matter. *Environmental Science & Technology*, *48*(17), 10098–10106. <https://doi.org/10.1021/es502670r>
- van der Sluijs, J., Kokelj, S. V., Fraser, R. H., Tunnicliffe, J., & Lacelle, D. (2018). Permafrost Terrain Dynamics and Infrastructure Impacts Revealed by UAV Photogrammetry and Thermal Imaging. *Remote Sensing*, *30*.
- St. Pierre, K. A., Zolkos, S., Shakil, S., Tank, S. E., St. Louis, V. L., & Kokelj, S. V. (2018). Unprecedented Increases in Total and Methyl Mercury Concentrations Downstream of Retrogressive Thaw Slumps in the Western Canadian Arctic. *Environmental Science & Technology*, *52*(24), 14099–14109. <https://doi.org/10.1021/acs.est.8b05348>
- Stubbins, A., Silva, L. M., Dittmar, T., & Van Stan, J. T. (2017). Molecular and Optical Properties of Tree-Derived Dissolved Organic Matter in Throughfall and Stemflow from Live Oaks and Eastern Red Cedar. *Frontiers in Earth Science*, *5*. <https://doi.org/10.3389/feart.2017.00022>
- Weishaar, J. L., Aiken, G. R., Bergamaschi, B. A., Fram, M. S., Fujii, R., & Mopper, K. (2003). Evaluation of Specific Ultraviolet Absorbance as an Indicator of the Chemical Composition and Reactivity of Dissolved Organic Carbon. *Environmental Science & Technology*, *37*(20), 4702–4708. <https://doi.org/10.1021/es030360x>
- Zolkos, S., Tank, S. E., & Kokelj, S. V. (2018). Mineral Weathering and the Permafrost Carbon-Climate Feedback. *Geophysical Research Letters*, *45*(18), 9623–9632. <https://doi.org/10.1029/2018GL078748>

